

So-ViT: Mind Visual Tokens for Vision Transformer

Jiangtao Xie¹, Ruiren Zeng¹, Qilong Wang², Ziqi Zhou³, Peihua Li¹

¹ Dalian University of Technology, ² Tianjin University, ³ MEGVII Technology

peihuali@dlut.edu.cn

Abstract

Recently the vision transformer (ViT) architecture, where the backbone purely consists of self-attention mechanism, has achieved very promising performance in visual classification. However, the high performance of the original ViT heavily depends on pretraining using ultra large-scale datasets, and it significantly underperforms on ImageNet-1K if trained from scratch. This paper makes the efforts toward addressing this problem, by carefully considering the role of visual tokens. First, for classification head, existing ViT only exploits class token while entirely neglecting rich semantic information inherent in high-level visual tokens. Therefore, we propose a new classification paradigm, where the second-order, cross-covariance pooling of visual tokens is combined with class token for final classification. Meanwhile, a fast singular value power normalization is proposed for improving the second-order pooling. Second, the original ViT employs the naive embedding of fixed-size image patches, lacking the ability to model translation equivariance and locality. To alleviate this problem, we develop a light-weight, hierarchical module based on off-the-shelf convolutions for visual token embedding. The proposed architecture, which we call So-ViT, is thoroughly evaluated on ImageNet-1K. The extensive results show our models, when trained from scratch, outperform the competing ViT variants, while being on par with or better than state-of-the-art CNN models.

1. Introduction

In the past years remarkable progress has been made in a wide variety of computer vision tasks such as visual recognition, object detection and semantic segmentation. This progress is primarily driven by significant advance of deep neural networks [19, 1], which learns varying levels of features by a stack of basic building blocks. In computer vision, the convolutional neural network (CNN) [36, 13, 16] is a dominating architecture underpinning from visual recognition to downstream tasks. Although the architecture of CNN has evolved significantly, the basic building block

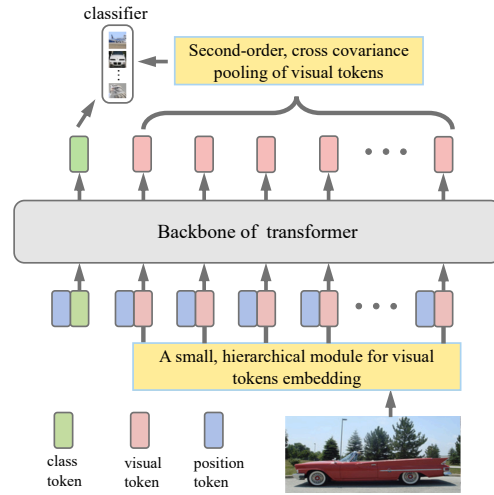


Figure 1: Diagram of our second-order vision transformer (So-ViT). We propose a classification paradigm, where the commonly used class token is combined with second-order, cross-covariance pooling of visual tokens. Meanwhile, we propose a singular value power normalization method to boost the performance of cross-covariance pooling. In addition, we develop a small, hierarchical module for effective embedding of visual tokens. Our model can address the downside of ViT [8], i.e., it *significantly underperforms when trained from scratch* on ImageNet-1K.

principally depends on convolutions [20].

Fundamentally different from CNN, the transformer architecture [39], which purely consists of the attention mechanism, has achieved great success in natural language processing (NLP). The attention mechanism can naturally learn long-range dependency and global context which CNNs struggle with, and so has attracted increasing interests of vision researchers. However, most of the methods for vision tasks focus on developing self-attention modules, inserted into the *backbones* of CNNs for improving performance. Until recently, the vision transformer (ViT) [8], where the backbone is constructed solely by a stack of trans-

former blocks, has achieved impressive performance for visual recognition. Unfortunately, on ImageNet-1K dataset, while being able to match or outperform state-of-the-art CNNs when pre-trained on ultra large-scale ImageNet-21K or JFT-300M datasets, the ViT models *significantly underperform if trained from scratch* [8].

Several reasons may account for this inferior performance. The classification paradigm of ViT follows the one that is commonly used in NLP [39]. That is, for *final classification*, ViT only utilizes the single class token while totally neglecting the visual tokens. We argue that visual tokens of high-level blocks contain rich semantic information and be helpful for classification. In addition, in ViT the visual tokens are embedded by a simple linear projection of fixed-size image patches, and then backbone invariably learns global relations of the resulting sequence of visual tokens. As such, unlike CNN, the ViT models contain no hierarchical structure, and lack the ability to learn the translation equivariance and local structure [8].

In light of the above two considerations, we present a novel architecture of ViT by modifying its classification head and the input embedding of visual tokens. For the classification head, we propose second-order, cross-covariance pooling of visual tokens as global image representation, which is combined with class token for final classification. Meanwhile, we design a light-weight, hierarchical module consisting of a stem and one stage for effective embedding of visual tokens. The visual tokens embeddings are then fed to the backbone of a stack of standard vision transformer blocks. Fig. 1 illustrates the proposed model, which we call second-order vision transformer (So-ViT).

Previous arts have shown that matrix power normalization (MPN) [40] plays a central role for the second-order representation. However, as our pooling method produces representations which are general square matrices (not necessarily symmetric or positive definite) or non-square ones, existing MPN and its fast algorithm cannot be applied. Inspired by MPN, we propose the singular value power normalization (svPN) method. The svPN can be implemented via singular value decomposition (SVD), which however is computationally expensive since SVD is unfriendly to GPU. We thus further develop an approximate normalization variant, which is very fast and effective.

Our contributions are summarized as follows.

- We propose a second-order vision transformer architecture. We introduce a classification paradigm which integrates visual tokens and class token. Meanwhile, we develop a small, hierarchical module for effective embedding of visual tokens.
- We present a singular value power normalization for general second-order representations. Furthermore, we develop an approximate normalization method, which is effective and very fast, suitable for large-scale

deep learning.

- We perform extensive experiments on ImageNet-1K for validating and evaluating our method. We are among the first to show that vision transformer can achieve compelling performance on ImageNet-1K when *trained from scratch*.

2. Related works

Transformer in the vision field The great success of the transformer architecture [39] has attracted ever-increasing interests in computer vision. The unique attention mechanism has found its applications in visual recognition and downstream vision tasks [11]. We can roughly divide the a multitude of works which concern attention mechanism into two categories. In the *first category*, varying self-attention modules are judiciously designed and inserted into the backbone of CNN for performance improvement [47, 41, 43]. These modules can capture global contextual knowledge, which can alleviate the disadvantage that the local receptive field is limited inherent in CNN. The *second category* studies whether the network backbone itself can be purely based on attention mechanism [3, 48]. Very recently, vision transformer (ViT) [8] has matched or surpassed state-of-the-art CNNs when trained on ultra large-scale datasets. However, the performance drops significantly if the ViT models are trained from scratch on ImageNet-1K. Several methods have been proposed to overcome this limitation [38, 44, 12]. DeiT [38] adopts knowledge distillation strategy for training the ViT model, where a distillation token is introduced to learn the knowledge from the teacher model. T2T-ViT [44] proposes a tokens-to-token module for embedding of visual tokens instead of the naive tokenization used in the original ViT. In TNT [12], a transformer-in-transformer block is proposed, where an outer and inner transformer blocks learn the dependency of inter- and intra-blocks, respectively. Our work is parallel to these ViT variants, but differently, we present a classification paradigm integrating second-order pooling of visual tokens and class token, and an effective embedding method for visual tokens.

Second-order pooling in CNN The second-order pooling (a.k.a. bilinear pooling), which generally produces symmetric positive definite (SPD) matrices as image representations, is a very active topic [46, 42]. The second-order pooling has been proven to be superior to the first-order, global average pooling in a number of visual tasks [24, 40]. Normalization plays a central role for improving the second-order representations. The bilinear CNN [26], motivated by Fisher Vector method [30], introduces element-wise power normalization followed by ℓ_2 normalization. DeepO₂P [17] exploits matrix logarithm normalization based on the Riemannian geometry of covariance matrices, which, however,

is harassed by numerical stability. Matrix power normalization (MPN) [22, 25] computes the power of the covariance matrix as image representation, performing significantly better than its counterparts. Particularly, Li et al. [40] disclose that MPN amounts to robust covariance estimation and meanwhile effectively exploits the geometric structure of covariance matrices. As MPN depends on eigen-decomposition which is GPU unfriendly, iSQRT [21] proposes a fast iterative method for computing matrix square root, suitable for parallel implementation on GPU. A recent study [31] has shown that MPN of second-order pooling improves Lipschitzness of the loss function, bringing about fast network acceleration and robustness to distorted images. In this paper, we study normalization for cross-covariance matrices which are general square or non-square and MPN can not be applied.

3. Second-order ViT architecture

We begin with an overview of the proposed So-ViT architecture (Sec. 3.1). Then we describe the cross-covariance pooling of visual tokens and how to combine with class token for classification (Sec. 3.2). Finally we introduce our visual token embedding method (Sec. 3.3).

3.1. Architecture overview

We present our Second-order ViT (So-ViT) architecture in Table 1. Given an input image, we design a light-weight module with a hierarchical structure accomplishing embedding of visual tokens. The module is a small network based on convolutions consisting of a stem and one stage. The convolution features from the embedding module are reshaped to a sequence of vectors as *visual tokens*.

As in [8], we prepend a learnable *class token* to the sequence of visual tokens, and then the position embeddings are added to retain positional information. The token sequence is fed to the backbone by stacking standard transformer blocks [8]. Every transformer block consists of a multi-head self-attention (MSA), and a multi-layer perceptron (MLP). Layer normalization and shortcut connection are applied before and after each transformer block, respectively. In each SA, the input features are linearly projected to the features called queries, keys and values, respectively, then the similarity matrix between the queries and keys are computed, and one finally computes the linear combination of values by multiplying the values with the similarity matrix (after softmax). The MLP contains two fully connected (FC) layers with a GELU nonlinearity following the first FC. Across the backbone, the token dimension, the head number, and the hidden layer dimension, denoted by p , h and p' , respectively, remains unchanged.

We combine visual tokens and class token for classification. We map the visual tokens to features of low dimension m and n by two separate linear projections. We then per-

	input size	structure	So-ViT-L
Head- classification paradigm	196×1	2 nd -order pooling	$\begin{bmatrix} \text{linear project, } m, n \\ \text{cross covariance} \\ \text{svPN} \\ \text{fully connected, 1000} \end{bmatrix}$
	1×1	class token	fully connected, 1000
backbone- stack of transformer blocks	197×1	$\begin{bmatrix} \text{MSA} \\ \\ \text{MLP} \end{bmatrix}$	$\begin{bmatrix} \text{linear project, } p/h \\ \text{similarity matrix} \\ \text{softmax} \\ \text{linear combination} \end{bmatrix} \times L$ $\begin{bmatrix} \text{fully connected, } p' \\ \text{fully connected, } p \end{bmatrix}$
Input- embedding of visual token	14×14	transition	conv, $1 \times 1, p$
	112×112	stage	$\begin{bmatrix} \text{conv, } 1 \times 1, 64 \\ \text{conv, } 3 \times 3, 64, S2 \\ \text{conv, } 1 \times 1, 256 \end{bmatrix} \times 3$
	224×224	stem	conv, $1 \times 1, 64$, max, S2

Table 1: Our So-ViT architecture. See text for details.

form cross-covariance pooling for the two branches of features, producing the second-order representation. The representation of visual tokens, after normalization via svPN, is integrated with that of the class token, fed to the final softmax classifier.

3.2. Fusing class and visual tokens for classification

The conventional classification paradigm of transformer models exclusively relies on class token, entirely discarding the visual tokens [8, 39]. We argue that high-level visual tokens contain rich semantic knowledge of the image, which are complementary to the class token. We thus propose second-order pooling for visual tokens, integrated with class token for classification.

Let $Z \in \mathbb{R}^{p \times N}$ be a matrix each column of which is the p -dimensional feature of a visual token. We perform two separate linear projections for the feature matrix Z , obtaining $X = W_1 Z$ and $Y = W_2 Z$, where $W_1 \in \mathbb{R}^{m \times p}$ and $W_2 \in \mathbb{R}^{n \times p}$ are learnable weight matrices. Without loss of generality, we suppose X and Y are both zero centered and $m \geq n$. We compute the *cross-covariance matrix* between X and Y , i.e., XY^T , followed by singular value power normalization as the second-order global image representation

$$Z' = \text{svPN}(XY^T). \quad (1)$$

Note that XY^T may be general square matrix (not symmetric or positive definite) or non-square matrix. As suggested by [40], normalization plays an important role for the global second-order pooling. However, matrix power normalization and its fast version [40] can only be used to SPD matrices. We propose singular value power normalization

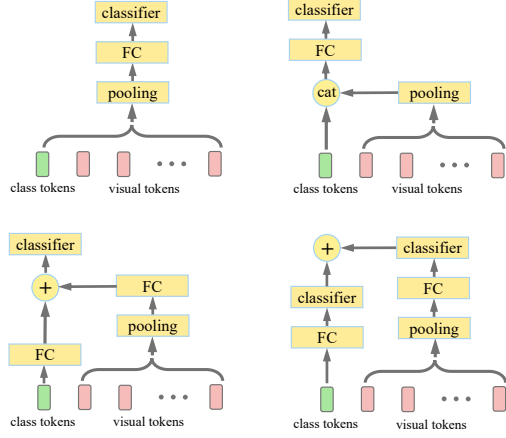


Figure 2: Illustration of different fusion schemes. Left top: aggregate; right top: concatenation; left bottom: sum at FC; right bottom: sum in loss.

(svPN) for the cross-covariance matrices. We defer details on motivation and method of svPN to next section.

Remark 1. Our second-order representation XY^T is different from the self-attention (SA) mechanism. The output of one SA which may take the form $(XY^T)W_3Z$ is basically a first-order representation, as it is a linear combination of input Z , where the coefficients of the linear combination is computed by the similarity matrix X^TY . Here W_3 is a learnable weight matrix.

We introduce several fusion schemes combining the class token and visual tokens, namely aggregate, sum and concatenation, as shown in Fig. 2. We propose to use cross-covariance pooling for the visual tokens. We mention that first-order, global average pooling can also be used [23, 36, 13]. For the aggregate scheme, we perform pooling for *all tokens*, right after the last transformer block (tran_L), and then consecutively connect to FC and softmax classifier. For the concatenation scheme, after tran_L , we concatenate the class token and the pooling result of visual tokens, and the concatenated representation is fed to FC and softmax classifier. For the sum scheme, we have two independent branches: one branch is the commonly used class token followed by FC, while the other branch, after pooling the visual tokens, connects to a separate FC. The outputs of the two FCs can be added and fed to one single softmax classifier. Alternatively, we can connect each FC to a separate softmax classifier and then add the two classification losses.

3.3. Embedding of visual tokens

The original ViT lacks the inductive bias of translation equivariance and locality, while relying on ultra large train-

ing data for combating this limitation [8]. A natural alternative is the hybrid model combining CNN and transformer. In [8], the convolution features from stage 4 of ResNet-50 is fed to the transformer model, making the hybrid model very heavy while gaining little. Our philosophy is different: *our idea* is a small hierarchical module for the purpose of visual token embedding, while the backbone still depends on transformer blocks.

Instead of the naive method by a linear projection of fixed-size patches in [8], we propose a lightweight, hierarchical module accomplishes visual token embedding. Our module is very simple, composed of a *stem* and a *stage*. The *stem* consists of a 3×3 convolution (conv) with 64 filters, followed a max pooling of stride 2 (S2). The succeeding *stage* contains a stack of 3 residual bottlenecks [13]. The middle 3×3 conv of each bottleneck has a stride of 2 for downsampling. To be compatible to the dimension of the follow-up transformer blocks, we exploit a transition layer of 1×1 conv with p channels. Each convolution layer is followed sequentially by a BN layer and ReLU layer. For an input image of $H \times W$ pixels, the output of our token embedding is feature maps with a spatial size of $H/8 \times W/8$ and p channels, where p is the dimension of the transformer blocks. By flattening the spatial dimensions, we obtain a sequence of $N = HW/64$ visual tokens of p -dimension.

The *stage* in our module is based on ResNet block. However, our choice is very flexible: we can also stack the Inception block [37], DenseNet block [16], or non-local block [41]. Our experiments (Sec. 5.1) show that these different choices perform favorably, all better than the competing method of T2T [44] for visual token embedding. This suggests that our idea of convolution based embedding matters, not the specific convolution blocks.

4. Normalization of cross-covariance matrix

We first describe the singular value power normalization svPN for cross-covariance matrices (Sec. 4.1). Next, we introduce an approximate svPN which is effective and fast (Sec. 4.2).

4.1. Singular value power normalization

Our method is motivated by MPN [40], an effective method for normalizing covariance matrix XX^T . It consists in calculating power of eigenvalues aligned with eigenvectors of the covariance matrix. The maximum variance formulation of principal component analysis [2, Chap. 12] states that, by consecutively projecting the random samples onto uncorrelated directions of principal components, we can sequentially obtain from the largest variance to the smallest variances. As the principal components/variances correspond to the eigenvectors/eigenvalues of covariance matrix, MPN can be statistically interpreted as *shrinking the variances aligned with the directions characterized by*

principal components. Taking a step further, we propose singular value normalization for the cross-covariance matrix XY^T .

We regard X and Y as two matrices consisting of N samples of random vector $x \in \mathbb{R}^m$ and $y \in \mathbb{R}^n$, respectively. Let $u \in \mathbb{R}^m$ and $v \in \mathbb{R}^n$ be two unit vectors, i.e., $\|u\| = \|v\| = 1$. We know that $R(Q, u, v) = u^T XY^T v$ is covariance of the projections of x on u and y on v , where $Q = XY^T$. The solution u_1 and v_1 to the objective $\max_{u,v, \|u\|=\|v\|=1} R(Q, u, v) = u^T XY^T v$ are the left and right singular vectors corresponding to the largest singular value $\lambda_1 = R(Q, u_1, v_1)$. Given u_k and v_k , $k \geq 1$, we maximize the objective $R(Q, u, v)$ with the constraints $u^T u_i = 0$ and $v^T v_i = 0$ for $i < k$, obtaining the left and right singular vectors u_k and v_k corresponding to the k -th largest singular value $\lambda_k = R(Q, u_k, v_k)$. The process of seeking largest cross-covariance between random vectors x and y amounts to singular value decomposition of Q . A proof of the above optimization process is given in the supplement. Motivated by MPN, we intend to *shrink the variances aligned with the left and singular vectors*, and define our normalization as

$$\text{svPN}(Q) = U \text{diag}(\lambda_i^\alpha) V^T = \sum_{i=1}^n \lambda_i^\alpha u_i v_i^T, \quad (2)$$

where $U = [u_1 \dots, u_n]$ and $V = [v_1 \dots, v_n]$ are orthonormal matrices, and $0 < \alpha < 1$.

Our svPN can be implemented accurately via SVD. Given an input matrix $Q \in \mathbb{R}^{m \times n}$, we first compute its SVD $Q = U \text{diag}(\lambda_i) V^T$ and then compute the normalized matrix $\tilde{Q} = U \text{diag}(\lambda_i^\alpha) V^T$. The two successive operations are described as

$$Q \xrightarrow{\text{SVD}} U \text{diag}(\lambda_i) V^T \xrightarrow{\text{power}} U \text{diag}(\lambda_i^\alpha) V^T \triangleq \tilde{Q}. \quad (3)$$

However, as the SVD algorithm is unfriendly to GPU, the above implementation is computationally expensive. In the next section, we will describe a fast method which performs normalization exploiting approximate singular values.

4.2. Approximate, fast singular value power normalization

Based on low rank assumption widely used in machine learning [10], we can efficiently implement approximate normalization by only estimating few largest singular values. We use the iterative method introduced in [34], which consecutively estimates the singular values in descending orders. Given an initial vector $v^{(0)}$, the iterative procedure takes the following form:

$$u^{(j+1)} = \frac{Q v^{(j)}}{\|Q v^{(j)}\|}, \quad v^{(k+1)} = \frac{Q^T u^{(j+1)}}{\|Q^T u^{(j+1)}\|}, \quad (4)$$

where the superscript denotes the iteration number. After several iterations, we achieve approximately the largest singular value $\hat{\sigma}_1 = \|Q^T u^{(j+1)}\|$ and the corresponding left and right singular vectors $\hat{u}_1 = u^{(j+1)}$, $\hat{v}_1 = v^{(j+1)}$, where the hat $\hat{\cdot}$ suggests they are approximate values. Suppose we have the k -th largest singular value, we deflate matrix Q to obtain

$$Q' = Q - \hat{\sigma}_k \hat{u}_k \hat{v}_k^T. \quad (5)$$

Then for deflated matrix Q' , we iterate using Eq. (4) achieving approximately the $(k+1)$ -th largest singular value $\hat{\sigma}_{k+1}$ and singular vectors $\hat{u}_{k+1}, \hat{v}_{k+1}$.

We can repeat the deflation (5) and the iteration (4). Suppose we have estimated r largest singular values. We define the approximate normalization as

$$\widehat{\text{svPN}}(Q) = \sum_{i=1}^{r-1} \hat{\sigma}_i^\alpha \hat{u}_i \hat{v}_i^T + \frac{1}{\sigma_r^{1-\alpha}} (Q - \sum_{i=1}^{r-1} \hat{\sigma}_i \hat{u}_i \hat{v}_i^T) \quad (6)$$

The rationale is that we shrink the 1st to $(r-1)$ -th singular values aligned with the corresponding singular vectors, while shrinking the remaining ones by using the r -th largest singular value.

5. Experiments

We first evaluate the proposed architecture of So-ViT (Sec. 5.1), followed by ablation study of singular value power normalization (Sec. 5.2). Then we conduct a comparison with T2T-ViT [44] which is closely related to our method (Sec. 5.3). Finally, we compare with state-of-the-art ViT variants and CNN models (Sec. 5.4). Our experiments are performed on large-scale ImageNet-1K benchmark [6], which contains 1.28 million training images and 50 thousands validation images. Our implementation is based on PyTorch framework and the models are trained with 8 NVIDIA 2080Ti GPUs.

We train the So-ViT models from scratch. We adopt standard scale, color and flip jittering for data augmentations [18, 13]. Following [44], we also adopt commonly used data augmentation techniques including mixup [14], randAugment [5] and cutmix [45], and label smoothing of value 0.1 [36]. We use AdamW [28] algorithm for network optimization with a batch of 512 and a weight decay of 0.05. The iteration starts with an initial learning rate of $1e-6$, increased to $5e-4$ (resp. $1e-3$) in three warmup epochs for models of 14 and 19 (resp. 7 and 10) transformer blocks. We use cosine annealing schedule whose final learning rate is $1e-5$ [27]. We use 310 training epochs as the transformer models require more iterations [8, 44, 12]. To facilitate extensive ablation analysis in Sec. 5.1 and Sec. 5.2, we use a shallow network containing 7 transformer blocks (i.e., So-ViT-7) with image resolution of 112×112 . For comparison

Stage of our embedding module	Top-1(%)	Params(M)	TFLOPs(G)	Speed(Hz)
T2T [44]	67.20	4.25	0.81	2133
ResNet block	70.40	4.28	0.88	2415
Inception block	69.48	4.09	0.81	2510
DenseNet block	70.39	4.23	1.06	1684
Non-local block	69.76	4.17	0.89	2098

Table 2: Comparison of embedding methods where the *stage* is based on varying type of convolution blocks. Only class token is used for classification.

with the state-of-the-art models, in Sec. 5.3 and Sec. 5.4, we adopt the conventional image resolution of 224×224 .

We design a family of models with varying number of transformer blocks L , i.e., So-ViT-7/10/14/19, where $p = 256/256/384/448$, $h = 4/4/6/7$, and $p' = 2p$ for the former two models and $p' = 3p$ for the latter two ones.

5.1. Evaluation of the So-ViT architecture

This section evaluates the proposed visual token embedding method and the classification paradigm which integrates the visual tokens with the class token.

Module of visual token embedding Our embedding module, as shown at the bottom of Tab. 1, is composed of a stem of 3×3 conv and one *stage* consisting of 3 residual blocks. The design of the stage can also be based on the Inception, DenseNet, or Non-local blocks. Due to limited space, the details of the embedding variants are given in the supplement. Tab. 2 compares different embedding modules and the T2T module [44]. We mention that the T2T module is a strong baseline, where soft-split operations are introduced in the transformer blocks right before the stack of transformer blocks for learning the local structure of visual tokens. Notably, all the convolution-based embedding modules outperform the T2T module by about 2% ~ 3%. The results suggest that our convolution based embedding method is very effective. This also suggests the potential to automatically design more advanced embedding methods (e.g., by neural architecture search [9]).

Fusion schemes for classification head Comparison of different fusion methods is presented in Tab. 3. We first note that all fusion schemes with 2nd-order pooling outperforms the baseline by about 2~4%, with moderate increase of parameters but without affecting TFLOPs; the scheme of sum (FC, 2nd) performs best, achieving 4.5% higher accuracy than the baseline. For fusion scheme with 1st-order pooling, the schemes of concat and sum (FC) are better than the baseline while the other two schemes are inferior to the baseline. As the dimension of the baseline representation (256-D) is less than that of the fusion method, for

Scheme	Pos	Pool	Dim	Top-1(%)	Params(M)	TFLOPs(G)
Baseline			256	70.40	4.28	0.88
(class token only)			2048	70.97	6.60	0.88
aggre	tran ₇	1st	256	68.69	4.28	0.88
		2nd	2048	74.58	6.10	0.88
concat	tran ₇	1st	512	71.23	4.54	0.88
		2nd	2304	74.41	6.36	0.88
sum	FC	1st	256	71.54	4.54	0.88
		2nd	2048	74.93	6.36	0.88
	loss	1st	256	70.33	4.54	0.88
		2nd	2048	73.36	6.36	0.88

Table 3: Results of different fusion schemes.

fair comparison, we add an additional linear projection for the baseline, increasing the dimension of the class token to 2048, which is called baseline+. We note that the baseline+ slightly improves over the baseline but still significantly lags behind the best fusion method (70.97 vs. 74.93). This indicates that the performance gains of the proposed method are mainly due to our classification paradigm (i.e., the fusion scheme) rather than simple increase of dimension.

From the analysis above, we have two observations. (1) Combination of visual tokens with class token for classification clearly performs much better than single class token, suggesting the effectiveness the proposed classification paradigm. (2) Compared to 1st-order pooling, the 2nd-order pooling achieves large gains, which suggests the the proposed cross-covariance pooling is very effective representation for the visual tokens.

5.2. Evaluation of svPN for second-order pooling

In this section, we evaluate the exact normalization (i.e., svPN) and the approximate one (i.e., \hat{svPN}). Subsequently, we compare the similarity matrix against the cross-covariance matrix. Then we assess the effect of the cross-covariance matrix size on performance. We finally compare different normalization methods.

Exact normalization v.s. approximate one Our normalization svPN can be implemented exactly by SVD which computes all singular values/vectors. The approximate method \hat{svPN} uses simple iteration algorithm for approximating few singular values/vectors. For svPN, the upper part of Table 4a shows the effect of exponent α (Eq. 2), where $\alpha = 0.5$ achieves the highest accuracy. However, svPN via SVD is computationally very expensive, running only at 110 Hz. In the lower part of Table 4a, setting $\alpha = 0.5$, we evaluate the effect of the number of singular values ($\#sv$) and the number of iterations ($\#iter$) on \hat{svPN} (Eq. 6). We note that overall the approximate normalization is slightly inferior to the accurate normaliza-

Method	Setting	Top-1	Speed (Hz)
svPN	α	0.3	74.86
		0.5	75.18
		0.7	74.91
$\widehat{\text{svPN}}$	(#sv, #iter) $\alpha = 0.5$	(1, 1)	74.93
		(1, 3)	75.03
		(1, 5)	73.71
		(2, 1)	73.12
		(3, 1)	74.67

(a) Exact normalization v.s. approximate normalization.

	Dim.	Top-1	Params (M)	TFLOPs (G)	Speed (Hz)
cross-cov	2048	74.93	6.36	0.88	2370
sim matrix	196 ²	70.01	42.78	0.94	2265

(b) Comparison of different second-order pooling methods.

Method	m	n	Dim	Top-1	Params (M)	TFLOPs (G)	Speed (Hz)
$\widehat{\text{svPN}}$	128	64	8K	77.13	12.53	0.90	2327
	64	64	4K	75.91	8.41	0.89	2349
	64	32	2K	74.93	6.36	0.88	2370
	48	24	1K	73.96	5.46	0.88	2393
	32	16	512	73.21	4.81	0.88	2415

(c) Effect of size of cross-covariance matrix.

	Method	Top-1
–	w/o normlization	73.88
$\frac{1}{\sqrt{N}}$	simple scaling	74.13
EPN	element-wise power normalization	71.31
LN	layer normalization	74.40
$\widehat{\text{svPN}}$	singular value power normalization	74.93

(d) Comparison with different normalization methods.

Table 4: Ablation analysis of svPN for second-order pooling.

tion. When using only the largest singular value, increase of iteration number brings insignificant gains. It is worth mentioning that similar phenomenon is also observed for the spectral normalization [29], where only one iteration is used to estimate the largest singular value for *weight normalization*. When we use two or three largest singular values, we observe performance decline. We conjecture that the reason is that estimation of the succeeding singular value/vectors are severely affected by the previous, inaccurate ones. Across the paper, we use $\widehat{\text{svPN}}$ with the single largest eigenvalue and one iteration for normalizing the second-order pooling.

Cross-covariance matrix v.s. similarity matrix As described in Sec. 3.2, we use cross-covariance matrix XY^T of visual tokens as the final image representation. Alternatively, the similarity matrix X^TY can be used. Here we compare the two different representations in Tab. 4b. It can be seen that the accuracy of similarity matrix is about 4.9% lower than the cross-covariance matrix. Note that the similarity matrix is spatial position dependent, which means that translation of objects in the image leads to different representation, hurtful for classification. In contrast, the cross-covariance matrix is a robust, position invariant representation, i.e., any permutation of visual tokens produce identical cross-covariance matrix.

Dimension of cross-covariance matrix The dimension of covariance matrix is $m \times n$, where m and n are dimensions of the two linear projections, as described in Sec. 3.2. Tab. 4c shows how the dimension (Dim) of cross-covariance matrix affect the performance. We can see that when the

dimension becomes larger, the accuracy consistently increases. When Dim=8K, the accuracy is 7.6% higher than the baseline which only uses class token (70.4%, Tab. 3). With Dim as small as 512, the result is still 2.8% higher than the baseline. Note that higher Dim leads to larger number of parameters, but very slight increase of computation. For performance-parameter trade-off, we choose Dim=2K across the paper, unless otherwise specified.

Comparison of different normalization methods We compare with element-wise power normalization (EPN), for which we tune the value of power, obtaining the value of 1/2 as the best hyperparameter. We also compare with layer normalization (LN) and a simple scaling method by dividing \sqrt{N} , where N is the number of visual tokens. We do not compare with MPN (or its faster vision iSQRT-COV), as the cross-covariance pooling produces general square or non-square matrices to which MPN can not be applied. The comparison results are given in Tab. 4d. We can see that all normalization methods improve over the baseline without normalization, suggesting the importance of normalization for the second-order pooling. Among all normalization methods, our $\widehat{\text{svPN}}$ performs best, achieving 0.5% higher top-1 accuracy than the second-best method, and improves about 1.1% over the baseline.

5.3. Comparison with T2T-ViT

Similar to our method, T2T-ViT proposes a T2T module for better token embedding, instead of the naive embedding method in the original ViT. So this section compares with this ViT variant and the results are presented in Tab. 5. As ResNet-50/101 have comparable computa-

Model	Top-1 (%)	Matching epochs	Params (M)	TFLOPs (G)	Speed (Hz)
T2T-ViT-7	71.2	–	4.2	0.9	1422
So-ViT-7	76.2	89(\downarrow_{221})	5.5	1.3	1414
T2T-ViT-10	74.1	–	5.8	1.2	1213
So-ViT-10	77.9	118(\downarrow_{192})	7.1	1.6	1191
ResNet-50*	79.1	–	25.5	4.3	800
T2T-ViT _t -14	80.7	–	21.5	5.2	385
So-ViT-14	81.8	188(\downarrow_{122})	24.6	4.6	607
ResNet-101*	79.9	–	44.6	7.9	488
T2T-ViT _t -19	81.4	–	39.0	8.4	278
So-ViT-19	82.4	176(\downarrow_{134})	43.8	8.1	367

Table 5: Comparison with T2T-ViT models. T2T-ViT_t and T2T-ViT respectively uses the transformer block [8] and its efficient variant [49]. *The results are duplicated from [44].

tion with So-ViT-14/19, we also list their results for reference. We first note that So-ViT and T2T-ViT are both significantly better than ResNet models. This suggests that the transformer models have stronger representation learning capability. In addition, our So-ViT consistently outperforms T2T-ViT by 1%~5% when both using same number of transformer blocks.

Next, we compare their convergence and speed. Overall, our models converge faster than T2T-ViT in that with remarkably less epochs, our So-ViT’s performance can match that of T2T-ViT trained with 310 epochs. For instance, T2T-ViT-14 achieves an accuracy of 80.7% with 310 epochs, while our model only requires 188 epochs to obtain the same accuracy. In particular, for shallower models our So-ViT converges even faster, e.g., So-ViT-7 with 89 epochs can attain the performance of T2T-ViT-7 trained with 310 epochs. For shallower models with 7/10 transformer blocks, our So-ViT has comparable speed with T2T-ViT which uses an efficient transformer block [49]. For deeper models with 14/17 blocks, our So-ViT runs 1.3x faster than T2T-ViT.

5.4. Comparison with state of the art

At last, we compare with state-of-the-art models which depend on the backbones of either ViT or CNN. For the ViT variants, we compare with T2T-ViT [44], DeiT [38] and TNT [12]. In the *upper part* of the Table 6, we compare with lite models aiming at mobile applications. We can see that So-ViT-7 achieves 2.1% higher accuracy than T2T-ViT-10 and the accuracy gap between So-ViT-10 and T2T-ViT-12 is about 2.4%. The *middle part* of Table 6 compares the models which have comparable computation with ResNet-50. It can be seen that our So-ViT-14 outperforms DeiT-S, T2T-ViT_t-14_t and TNT-S by about 2.0%, 1.1% and 0.5%, respectively. By combining the SE block [15], the accuracy of TNT-S increases but is still lower than ours. As shown in the *bottom part* of Table 6, our So-ViT-19 performs better than T2T-ViT-19 by 1.0%; TNT-B achieves higher accuracy

Backbone	Model	Top-1 (%)	Params(M)	TFLOPs(G)
CNN	MobileNetV2 1.0x* [33]	72.8	3.5	0.3
	MobileNetV2 1.4x* [33]	75.6	6.9	0.6
	RegNetX-400MF [32]	72.7	5.2	0.4
	RegNetX-600MF [32]	74.1	6.2	0.6
	RegNetX-800MF [32]	75.2	7.3	0.8
ViT	T2T-ViT-7 [44]	71.2	4.2	0.9
	T2T-ViT-10 [44]	74.1	5.8	1.2
	T2T-ViT-12 [44]	75.5	6.8	1.4
	So-ViT-7 (ours)	76.2	5.5	1.3
	So-ViT-10 (ours)	77.9	7.1	1.6
CNN	ResNet-50 [13]	76.2	25.5	4.3
	Xception [4]	79.0	22.9	8.4
	Inception-v3 [37]	78.8	23.6	5.7
	DenseNet-264 [16]	77.9	34.8	6.0
ViT	DeiT-S [38]	79.8	22.1	4.6
	T2T-ViT _t -14 [44]	80.7	21.5	5.2
	TNT-S [12]	81.3	23.8	5.2
	TNT-S+SE [12]	81.6	24.7	5.2
	So-ViT-14 (ours)	81.8	24.6	4.6
CNN	ResNet101 [13]	77.4	44.6	7.9
	Inception-v4 [35]	80.0	48.0	13.0
	RegNetX-8.0GF [32]	79.3	39.6	8.0
	RepVGG-B2g4 [7]	79.4	55.8	11.3
ViT	DeiT-B [38]	81.8	86.4	17.6
	TNT-B [12]	82.8	65.6	14.1
	ViT-S/16 [8]	78.1	48.6	10.1
	T2T-ViT-19 [44]	81.2	39.0	8.0
	T2T-ViT _t -19 [44]	81.4	39.0	8.4
	So-ViT-19 (ours)	82.4	43.8	8.1

Table 6: Comparison with state-of-the-art models. *The results are duplicated from [44].

than ours but its parameter and TFLOPs are considerably larger. Finally, we note that the proposed So-ViT models perform on par or better than state-of-the-art CNN models, either for lite network focusing on the mobile environment, or complex, deeper models aiming at high performance.

6. Conclusion

We propose a second-order vision transformer (So-ViT) model for image classification. For the network head, we propose integration of cross-covariance pooling of visual tokens with class token fed to classifier. As far as we know, this is the first attempt to exploit high-level visual features in the transformer architecture for final classification. For the network input, we design a small hierarchical module for effective visual token embedding, based on off-the-shelf convolutions. Extensive experiments have shown that our So-ViT models are very competitive, compared to state-of-the-art ViT models and CNN models. The effectiveness of our idea for visual token embedding suggests that it is promising to automatically seek the embedding module by NAS [9]. In the future, we are interested to study how our So-ViT will perform for the tasks of NLP [39].

References

- [1] Yoshua Bengio, Aaron Courville, and Pascal Vincent. Representation learning: A review and new perspectives. *IEEE TPAMI*, 35(8):1798–1828, 2013. 1
- [2] Christopher Bishop. *Pattern Recognition and Machine Learning*. Springer, 2006. 4
- [3] Nicolas Carion, Francisco Massa, Gabriel Synnaeve, Nicolas Usunier, Alexander Kirillov, and Sergey Zagoruyko. End-to-end object detection with transformers. In *ECCV*, 2020. 2
- [4] François Chollet. Xception: Deep learning with depthwise separable convolutions. In *CVPR*, 2017. 8
- [5] Ekin D Cubuk, Barret Zoph, Jonathon Shlens, and Quoc V Le. Randaugment: Practical automated data augmentation with a reduced search space. In *CVPR*, 2020. 5
- [6] Jia Deng, Wei Dong, Richard Socher, Li-Jia Li, Kai Li, and Li Fei-Fei. ImageNet: A large-scale hierarchical image database. In *CVPR*, 2009. 5
- [7] Xiaohan Ding, Xiangyu Zhang, Ningning Ma, Jungong Han, Guiguang Ding, and Jian Sun. Repvgg: Making vgg-style convnets great again. *arXiv:2101.03697*, 2021. 8
- [8] Alexey Dosovitskiy, Lucas Beyer, Alexander Kolesnikov, Dirk Weissenbor, Xiaohua Zhai, Thomas Unterthiner, Mostafa Dehghani, Matthias Minderer, Georg Heigold, Sylvain Gelly, Jakob Uszkoreit, and Neil Houlsby. An image is worth 16x16 words: Transformers for image recognition at scale. In *ICLR*, 2021. 1, 2, 3, 4, 5, 8
- [9] Thomas Elsken, Jan Hendrik Metzen, and Frank Hutter. Neural architecture search: A survey. *JMLR*, 2019. 6, 8
- [10] Arthur Gretton, Michael W Mahoney, Mehryar Mohri, and Ameet S Talwalkar. *NIPS2010 Workshop*. 2010. 5
- [11] Kai Han, Yunhe Wang, Hanting Chen, Xinghao Chen, Jianyuan Guo, Zhenhua Liu, Yehui Tang, An Xiao, Chunjing Xu, Yixing Xu, Zhaohui Yang, Yiman Zhang, and Dacheng Tao. A survey on visual transformer. *arXiv:2012.12556v3*, 2020. 2
- [12] Kai Han, An Xiao, Enhua Wu, Jianyuan Guo, Chunjing Xu, and Yunhe Wang. Transformer in transformer. *arXiv:2103.00112*, 2021. 2, 5, 8
- [13] Kaiming He, Xiangyu Zhang, Shaoqing Ren, and Jian Sun. Deep residual learning for image recognition. In *CVPR*, 2016. 1, 4, 5, 8
- [14] Yann N. Dauphin David Lopez-Paz Hongyi Zhang, Moustapha Cisse. mixup: Beyond empirical risk minimization. *ICLR*, 2018. 5
- [15] Jie Hu, Li Shen, and Gang Sun. Squeeze-and-excitation networks. In *CVPR*, 2018. 8
- [16] Gao Huang, Zhuang Liu, Laurens Van Der Maaten, and Kilian Q Weinberger. Densely connected convolutional networks. In *CVPR*, 2017. 1, 4, 8
- [17] Catalin Ionescu, Orestis Vantzos, and Cristian Sminchisescu. Matrix backpropagation for deep networks with structured layers. In *ICCV*, 2015. 2
- [18] Andrew Zisserman Karen Simonyan. Very deep convolutional networks for large-scale image recognition. In *ICLR*, 2015. 5
- [19] Yann LeCun, Yoshua Bengio, and Geoffrey Hinton. Deep learning. *Nature*, 2015. 1
- [20] Y. Lecun, L. Bottou, Y. Bengio, and P. Haffner. Gradient-based learning applied to document recognition. *Proceedings of the IEEE*, pages 2278–2324, 1998. 1
- [21] Peihua Li, Jiangtao Xie, Qilong Wang, and Zilin Gao. Towards faster training of global covariance pooling networks by iterative matrix square root normalization. In *CVPR*, 2018. 3
- [22] Peihua Li, Jiangtao Xie, Qilong Wang, and Wangmeng Zuo. Is second-order information helpful for large-scale visual recognition? In *ICCV*, 2017. 3
- [23] M. Lin, Q. Chen, and S. Yan. Network in network. In *ICLR*, 2014. 4
- [24] Tsung-Yu Lin, Aruni Roy Chowdhury, and Subhransu Maji. Bilinear convolutional neural networks for fine-grained visual recognition. *IEEE TPAMI*, 40(6):1309–1322, 2018. 2
- [25] Tsung-Yu Lin and Subhransu Maji. Improved bilinear pooling with CNNs. In *BMVC*, 2017. 3
- [26] Tsung-Yu Lin, Aruni Roy Chowdhury, and Subhransu Maji. Bilinear CNN models for fine-grained visual recognition. In *ICCV*, 2015. 2
- [27] Ilya Loshchilov and Frank Hutter. Sgdr: stochastic gradient descent with warm restarts. In *ICLR*, 2017. 5
- [28] Ilya Loshchilov and Frank Hutter. Decoupled weight decay regularization. In *ICLR*, 2018. 5
- [29] Takeru Miyato, Toshiki Kataoka, Masanori Koyama, and Yuichi Yoshida. Spectral normalization for generative adversarial networks. In *ICLR*, 2018. 7
- [30] Florent Perronnin, Jorge Sánchez, and Thomas Mensink. Improving the fisher kernel for large-scale image classification. In *ECCV*, 2010. 2
- [31] Banggu Wu Dongwei Ren Peihua Li Wangmeng Zuo Qinghua Hu Qilong Wang, Li Zhang. What deep cnns benefit from global covariance pooling: An optimization perspective. In *CVPR*, 2020. 3
- [32] Ilija Radosavovic, Raj Prateek Kosaraju, Ross Girshick, Kaiming He, and Piotr Dollár. Designing network design spaces. In *CVPR*, 2020. 8
- [33] Mark Sandler, Andrew Howard, Menglong Zhu, Andrey Zhmoginov, and Liang-Chieh Chen. Mobilenetv2: Inverted residuals and linear bottlenecks. In *CVPR*, 2018. 8
- [34] Seymour Shlien. A method for computing the partial singular value decomposition. *IEEE TPAMI*, 1982. 5
- [35] Christian Szegedy, Sergey Ioffe, Vincent Vanhoucke, and Alexander Alemi. Inception-v4, inception-resnet and the impact of residual connections on learning. In *AAAI*, volume 31, 2017. 8
- [36] Christian Szegedy, Wei Liu, Yangqing Jia, Pierre Sermanet, Scott Reed, Dragomir Anguelov, Dumitru Erhan, Vincent Vanhoucke, and Andrew Rabinovich. Going deeper with convolutions. In *CVPR*, 2015. 1, 4, 5
- [37] Christian Szegedy, Vincent Vanhoucke, Sergey Ioffe, Jon Shlens, and Zbigniew Wojna. Rethinking the inception architecture for computer vision. In *CVPR*, 2016. 4, 8
- [38] Hugo Touvron, Matthieu Cord, Matthijs Douze, Francisco Massa, Alexandre Sablayrolles, and Hervé Jégou. Training data-efficient image transformers & distillation through attention. *arXiv:2012.12877*, 2020. 2, 8

- [39] Ashish Vaswani, Noam Shazeer, Niki Parmar, Jakob Uszkoreit, Llion Jones, Aidan N Gomez, Lukasz Kaiser, and Illia Polosukhin. Attention is all you need. In *NIPS*, 2017. 1, 2, 3, 8
- [40] Qilong Wang, Jiangtao Xie, Wangmeng Zuo, Lei Zhang, and Peihua Li. Deep CNNs meet global covariance pooling: Better representation and generalization. *IEEE TPAMI*, 2020. 2, 3, 4
- [41] Xiaolong Wang, Ross Girshick, Abhinav Gupta, and Kaiming He. Non-local neural networks. In *CVPR*, 2018. 2, 4
- [42] Zhengyang Wang and Shuiwang Ji. Second-order pooling for graph neural networks. *IEEE TPAMI*, page 1, 2020. 2
- [43] CSanghyun Woo, Jongchan Park, Joon-Young Lee, and In So Kweon. BAM: Convolutional block attention module. In *ECCV*, 2018. 2
- [44] Li Yuan, Yunpeng Chen, Tao Wang, Weihao Yu, Yujun Shi, Francis Tay, Jiashi Feng, and Shuicheng Yan. Tokens-to-token ViT: Training vision transformers from scratch on imagenet, 2021. 2, 4, 5, 6, 8
- [45] Sangdoo Yun, Dongyoon Han, Seong Joon Oh, Sanghyuk Chun, Junsuk Choe, and Youngjoon Yoo. Cutmix: Regularization strategy to train strong classifiers with localizable features. In *ICCV*, 2019. 5
- [46] Jianjia Zhang, Lei Wang, Luping Zhou, and Wanqing Li. Beyond covariance: SICE and kernel based visual feature representation. *IJCV*, 2021. 2
- [47] Hengshuang Zhao, Jiaya Jia, and Vladlen Koltun. Exploring self-attention for image recognition. In *CVPR*, 2020. 2
- [48] Sixiao Zheng, Jiachen Lu, Hengshuang Zhao, Xiatian Zhu, Zekun Luo, Yabiao Wang, Yanwei Fu, Jianfeng Feng, Tao Xiang, Philip HS Torr, and Li Zhang. Rethinking semantic segmentation from a sequence-to-sequence perspective with transformers. *arXiv:2012.15840*, 2020. 2
- [49] Yiming Yang Kris Kitani Zhiqing Sun, Shengcao Cao. Rethinking transformer-based set prediction for object detection. *arXiv:2011.10881*, 2020. 8

Supplementary

In this supplement, we first prove that the optimization process of seeking largest cross-covariance amounts to singular value decomposition (SVD). We then give the back-propagation formulas associated with svPN and the approximate normalization $\hat{\text{svPN}}$. Next, we provide implementation details on different visual token embedding modules. Finally, we provide additional experiments to further evaluate the proposed methods.

A. Maximum cross-covariance analysis

Let $X \in \mathbb{R}^{m \times N}$ and $Y \in \mathbb{R}^{n \times N}$ be two matrices consisting of N samples of random vector $x \in \mathbb{R}^m$ and $y \in \mathbb{R}^n$, respectively. Without loss of generality, we assume X and Y are both zero centered by subtracting the mean of each row. Then $Q = XY^T$ is the cross-covariance matrix¹ between x and y [S-5]. Let u and v be unit vectors, i.e., $\|u\| = \|v\| = 1$, where $\|\cdot\|$ is the Euclidean norm. $R(Q, u, v) = u^T XY^T v$ is the (cross-)covariance between the projections of x on u and that of y on v . Let us consider how to seek *a series of u and v aligned which we obtain consecutively the largest cross-covariances between x and y* . In the main manuscript, we state that such a process, which is now described in Proposition 1, amounts to singular value decomposition of Q . We call this optimization process *maximum cross-covariance analysis (MCA)*.

Proposition 1. *Consider the objective*

$$\begin{aligned} \max_{u,v} R(Q, u, v) &= u^T Q v \\ \text{s.t. } \|u\| &= 1, \|v\| = 1. \end{aligned} \quad (\text{S-1})$$

The solution u_1 and v_1 to the objective S-1 are respectively left and right singular vectors corresponding to the largest singular value $\lambda_1 = R(Q, u_1, v_1)$ of matrix Q . We can repeat this process. Given u_i and v_i , $i = 1, \dots, k-1$, we optimize the objective

$$\begin{aligned} \max_{u,v} R(Q, u, v) &= u^T XY^T v \\ \text{s.t. } \|u\| &= 1, \|v\| = 1, \\ u_i^T u &= 0, v_i^T v = 0, i < k. \end{aligned} \quad (\text{S-2})$$

The vectors u_k and v_k which maximize the objective S-2 are respectively left and right singular vectors corresponding to the k -th largest singular value $\lambda_k = R(Q, u_k, v_k)$ of Q . The optimization process produces $R(Q, u_1, v_1) \geq \dots \geq R(Q, u_{k-1}, v_{k-1}) \geq R(Q, u_k, v_k)$, where $R(Q, u_i, v_i)$ is the i -th largest singular value of Q while u_i and v_i are the

¹The cross-covariance matrix is often estimated as $P = \frac{1}{N}XY^T$; for notational simplicity, we omit the constant $\frac{1}{N}$ which does not affect our analysis.

corresponding left and right singular vectors, respectively. Therefore, the optimization process above amounts to SVD of Q .

Proof. We will prove this proposition using *mathematical induction*. We use the method of Lagrange multipliers to solve the constrained optimization problems.

Initial case Note that $\|u\| = 1$ is equivalent to $\|u\|^2 = u^T u = 1$ as the inner product has the property of non-negativity. The Lagrange function associated with the objective S-1 is

$$\mathcal{L}(u, v, \gamma, \beta) = R(Q, u, v) - \frac{\gamma}{2}(u^T u - 1) - \frac{\beta}{2}(v^T v - 1). \quad (\text{S-3})$$

We calculate the gradient $\nabla \mathcal{L} = \left[\frac{\partial \mathcal{L}}{\partial u}, \frac{\partial \mathcal{L}}{\partial v}, \frac{\partial \mathcal{L}}{\partial \gamma}, \frac{\partial \mathcal{L}}{\partial \beta} \right]$, where $\frac{\partial \mathcal{L}}{\partial u}$ is the partial derivatives of \mathcal{L} with respect to u , and set it to be zero. After some manipulations, we have

$$\begin{aligned} Qv - \gamma u &= 0, \\ Q^T u - \beta v &= 0, \\ u^T u - 1 &= 0, \\ v^T v - 1 &= 0. \end{aligned} \quad (\text{S-4})$$

The last two equations simply produce the constraints, i.e., $\|u\| = 1$ and $\|v\| = 1$. We left multiple the first and second equation by u^T and v^T , respectively. Then we can obtain

$$\gamma = \beta = R(Q, u, v),$$

as $u^T Qv = v^T Qu$. Therefore, we have

$$\begin{aligned} Qv &= \gamma u, \\ Q^T u &= \gamma v. \end{aligned} \quad (\text{S-5})$$

According to the property of SVD [S-4, Chap 2.4], we know that u and v which satisfy S-5 are respectively left and right singular vectors of Q with γ being the singular value. Obviously, $R(Q, u, v)$ achieves its maximum when it is equal to the largest singular value. Therefore, by optimizing the objective S-1, we obtain vectors u_1 and v_1 which are respectively the left and right singular vectors corresponding to the largest singular value $\lambda_1 = R(Q, u_1, v_1)$.

Inductive step Suppose that the statement associated with the objective S-2 holds for $i < k$. That is, for any i , u_i and v_i , which maximize $R(Q, u, v)$ while satisfying the constraints $\|u_i\| = \|v_i\| = 1$ and $u_i^T u_{i'} = 0, v_i^T v_{i'} = 0, i' < i$, are the singular vectors corresponding to the i th largest singular values λ_i . Obviously

$$\underbrace{R(Q, u_1, v_1)}_{\lambda_1} \geq \dots \geq \underbrace{R(Q, u_{k-1}, v_{k-1})}_{\lambda_{k-1}}.$$

Now, let us prove the statement holds for the case k .

The Lagrange function associated with the objective (S-2) is

$$\mathcal{L}(u, v, \gamma, \beta, \tau_i, \delta_i) = R(Q, u, v) - \frac{\gamma}{2}(u^T u - 1) - \frac{\beta}{2}(v^T v - 1) - \sum_{i=1}^{k-1} \tau_i u^T u_i - \sum_{i=1}^{k-1} \delta_i v^T v_i. \quad (\text{S-6})$$

We calculate the gradient of the Lagrange function $\nabla \mathcal{L} = \left[\frac{\partial \mathcal{L}}{\partial u}, \frac{\partial \mathcal{L}}{\partial v}, \frac{\partial \mathcal{L}}{\partial \gamma}, \frac{\partial \mathcal{L}}{\partial \beta}, \frac{\partial \mathcal{L}}{\partial \tau_1}, \dots, \frac{\partial \mathcal{L}}{\partial \tau_{k-1}}, \frac{\partial \mathcal{L}}{\partial \delta_1}, \dots, \frac{\partial \mathcal{L}}{\partial \delta_{k-1}} \right]$. By setting the gradient $\nabla \mathcal{L}$ to be zero, we obtain a set of equations

$$\begin{aligned} Qv - \gamma u - \sum_{i=1}^{k-1} \tau_i u_i &= 0, \\ Q^T u - \beta v - \sum_{i=1}^{k-1} \delta_i v_i &= 0, \\ u^T u - 1 &= 0, \\ v^T v - 1 &= 0, \\ u^T u_i &= 0, \quad i = 1, \dots, k-1, \\ v^T v_i &= 0, \quad i = 1, \dots, k-1. \end{aligned} \quad (\text{S-7})$$

The third to last equations are simply constraints of the maximization problem S-2. We left multiply u^T (resp. v^T) the first (resp. second) equation, and we can obtain $u^T Qv = \gamma$ (resp. $v^T Q^T u = \beta$), by noting that $u^T u_i = 0$ (resp. $v^T v_i = 0$) u for $i < k$. Therefore, we have $\gamma = \beta = R(Q, u, v)$.

Subsequently, we will show that $\tau_j = 0, j < k$. We left multiply the first equation by $u_j^T, j < k$. We recall that u_j is orthogonal to $u_{j'}$ for $j' \neq j$ and to u , and then can derive

$$\tau_j = u_j^T Qv.$$

As u_j is the left singular value of Q , we know $Q^T u_j = \lambda_j v_j$, i.e., $u_j^T Q = \lambda_j v_j^T$. Therefore we have

$$\tau_j = u_j^T Qv = \lambda_j v_j^T v = 0.$$

Here we make use of the fact that v_j is orthogonal to v . In a similar manner, we left multiply the second equation by $v_j^T, j < k$, and then we can derive $\delta_j = 0$. Up to this point, we know u and v for which the objective S-2 is maximized satisfy the following pair of equations

$$\begin{aligned} Qv &= \gamma u, \\ Q^T u &= \gamma v. \end{aligned} \quad (\text{S-8})$$

Again, according to the property of SVD, we know u and v are left and right singular values of Q and γ is the corresponding singular value. Obviously, γ achieves the maximum when it equals the k th largest singular value. This concludes our proof. \square

As far as we know, the statement as described in Proposition 1 appeared early in [S-3] and later in [S-13, Chap. 14.1.7], among others. However, we fail to find any formal proof of this statement and thus we give one in this supplemental material. It is worth mentioning that MCA is closely related to but different from canonical correlation analysis (CCA). For detailed theory on CCA, one may refer to [S-12].

In terms of MCA, we propose to normalize the second-order representation $Q = XY^T$ by shrinking the maximum cross-covariance of random vectors x and y aligned with the associated pairs of vectors, which is equivalent to shrinking the singular values aligned with the corresponding singular vectors of Q . We are motivated by MPN [S-14], which normalizes $P = XX^T$ by shrinking the eigenvalues aligned with the corresponding eigenvectors of P ; it can be interpreted as, based on maximum variance analysis of principal component analysis (PCA) [S-2, Chap. 12], shrinkage of the maximum variances of random vector x aligned with the associated, principal components. Our normalization method is a natural generalization of MPN.

B. Backpropagation of singular value power normalization

We give the backpropagation formulas for the exact singular value power normalization (i.e., svPN) and for the approximate one (i.e., $\widehat{\text{svPN}}$).

B.1. Backpropagation of svPN

Let $Q = U \text{diag}(\lambda_i) V^T$ be the SVD of Q . The forward propagation of our normalization can be described in two consecutive steps as follows:

$$\text{svPN} : Q \xrightarrow{\text{SVD}} U \text{diag}(\lambda_i) V^T \xrightarrow{\text{power}} U \text{diag}(\lambda_i^\alpha) V^T \triangleq \tilde{Q} \quad (\text{S-9})$$

The associated backward propagations are not straightforward as the structured, nonlinear matrix operations are involved. Suppose l is the network loss function. Let us denote $A_{\text{sym}} = \frac{1}{2}(A + A^T)$, $\Lambda = \text{diag}(\lambda_i)$, and A_{diag} being a matrix setting the off-diagonals of A to zero. Based on the theory of matrix backpropagation [S-8], we can derive the gradients relative to svPN via SVD, which are given in the following corollary.

Remark 2. Suppose we have $\frac{\partial l}{\partial \tilde{Q}}$ from the succeeding layer. The gradient involved in the first step of S-9 is

$$\begin{aligned} \frac{\partial l}{\partial Q} &= \frac{\partial l}{\partial U} \Lambda^{-1} V^T + U \left(\frac{\partial l}{\partial \Lambda} - U^T \frac{\partial l}{\partial U} \Lambda^{-1} \right)_{\text{diag}} V^T \\ &\quad + 2U \Lambda \left(K^T \circ \left(V^T \left(\frac{\partial l}{\partial V} - V \Lambda^{-1} \left(\frac{\partial l}{\partial U} \right)^T U \Lambda \right) \right) \right)_{\text{sym}} V^T \end{aligned}$$

where $K_{ij} = (\lambda_i^2 - \lambda_j^2)^{-1}$ if $\lambda_i \neq \lambda_j$ and $K_{ij} = 0$ otherwise, and \circ denotes Hadamard product. The partial derivatives with respect to the second step of S-9 are

$$\begin{aligned}\frac{\partial l}{\partial U} &= \frac{\partial l}{\partial \tilde{Q}} V \Lambda^\alpha, \\ \frac{\partial l}{\partial V} &= \left(\frac{\partial l}{\partial \tilde{Q}} \right)^T U \Lambda^\alpha, \\ \frac{\partial l}{\partial \Lambda} &= \alpha \Lambda^{\alpha-1} U^T \frac{\partial l}{\partial \tilde{Q}} V.\end{aligned}$$

B.2. Backpropagation of $\hat{\text{svPN}}$

In the approximate normalization $\hat{\text{svPN}}$, we only compute several dominant singular values through the iteration method. The forward propagation mainly involves repeated estimation of approximate singular value/vectors and matrix deflation. The estimation of approximate singular value and singular vectors depends on iterations of a pair of equations (for notational simplification, we omit the iteration index) like the following

$$u = \frac{Qv}{\|Qv\|}, \quad v = \frac{Q^T u}{\|Q^T u\|}. \quad (\text{S-10})$$

Since the deflation operation contains only simple linear matrix addition and multiplication, it is easy to derive the gradient involved and so we omit the derivation. The following corollary gives the backpropagation formulas of the first equation in S-10, while that of the second equation has similar form and is left out.

Remark 3. For $u = \frac{Qv}{\|Qv\|}$, given $\frac{\partial l}{\partial u}$ passed from the succeeding layer, the partial derivatives of the loss function l with respect to Z and v are

$$\begin{aligned}\frac{\partial l}{\partial Z} &= \frac{1}{\|Zv\|} \frac{\partial l}{\partial u} v^T - \frac{1}{\|Zv\|^3} \text{tr} \left(Zv \left(\frac{\partial l}{\partial u} \right)^T \right) Z v v^T, \\ \frac{\partial l}{\partial v} &= \frac{1}{\|Zv\|} Z^T \frac{\partial l}{\partial u} - \frac{1}{\|Zv\|^3} \text{tr} \left(Zv \left(\frac{\partial l}{\partial u} \right)^T \right) Z^T Z v,\end{aligned}$$

where $\text{tr}(\cdot)$ denotes matrix trace.

Once we have estimated r largest singular values $\hat{\sigma}_i$ and the corresponding singular vectors \hat{u}_i and \hat{v}_i , we can perform approximate singular value power normalization

$$\hat{\text{svPN}} : \tilde{Q} = \sum_{i=1}^{r-1} \hat{\sigma}_i^\alpha \hat{u}_i \hat{v}_i^T + \frac{1}{\sigma_r^{1-\alpha}} \left(Q - \sum_{i=1}^{r-1} \hat{\sigma}_i \hat{u}_i \hat{v}_i^T \right). \quad (\text{S-11})$$

The backpropagation formulas related to S-11 are given in the corollary as follows.

Remark 4. Given $\frac{\partial l}{\partial \tilde{Q}}$ passed from the succeeding layer, the partial derivatives of l involved in S-11 are

$$\begin{aligned}\frac{\partial l}{\partial \hat{\sigma}_i} &= \left(\alpha \hat{\sigma}_i^{\alpha-1} - \hat{\sigma}_r^{\alpha-1} \right) \text{tr} \left(\left(\frac{\partial l}{\partial \tilde{Q}} \right)^T \hat{u}_i \hat{v}_i^T \right), \\ \frac{\partial l}{\partial \hat{u}_i} &= \hat{\sigma}_i \left(\hat{\sigma}_i^{\alpha-1} - \hat{\sigma}_r^{\alpha-1} \right) \frac{\partial l}{\partial \tilde{Q}} \hat{v}_i, \\ \frac{\partial l}{\partial \hat{v}_i} &= \hat{\sigma}_i \left(\hat{\sigma}_i^{\alpha-1} - \hat{\sigma}_r^{\alpha-1} \right) \left(\frac{\partial l}{\partial \tilde{Q}} \right)^T \hat{u}_i, \\ \frac{\partial l}{\partial \hat{\sigma}_r} &= \left(\alpha - 1 \right) \hat{\sigma}_r^{\alpha-2} \text{tr} \left(\left(\frac{\partial l}{\partial \tilde{Q}} \right)^T \left(Q - \sum_{i=1}^{r-1} \hat{\sigma}_i \hat{u}_i \hat{v}_i^T \right) \right), \\ \frac{\partial l}{\partial Q} &= \hat{\sigma}_r^{\alpha-1} \frac{\partial l}{\partial \tilde{Q}},\end{aligned}$$

where $i = 1, \dots, r-1$.

Though popular deep learning libraries such as PyTorch [S-10] and TensorFlow [S-1] provide automatic differentiation (autodiff) engine, some widely used frameworks (e.g., Caffe [S-9]) have no autodiff and so for implementation we need to derive explicitly the backpropagation formulas. Moreover, given the explicit gradients, one can manually optimize the implementation, which may be more efficient than the implementation based on the mechanical autodiff.

C. Implementation details on embedding modules

Our embedding module is a light-weight, hierarchical structure, consisting of a *stem* and a *stage*. The *stem* contains only one 3×3 convolution (conv) followed by a max pooling of stride 2 (S2), while the *stage* consists of a stack of convolution blocks. The design of the stage is flexible, which can be based on different type of convolution blocks. The details on configurations of ResNet block (i.e., residual bottleneck) [S-6], Inception block [S-11], DenseNet block [S-7] and non-local block [S-15] proposed for our stage are shown in Fig. S-3.

For the stage respectively based on ResNet, Inception and DenseNet, a stack of 3 convolution blocks are employed. A BN layer and a ReLU layer are inserted after each convolution for the ResNet block and Inception block, but before each convolution for the DenseNet block. Specifically, every DenseNet block contains 6 bottleneck structures of BN-ReLU-conv(1×1)-BN-ReLU-conv(3×3), followed by a 1×1 convolution and 2×2 average pooling with a stride of 2. For the stage based on Non-local network, we stack 2 Non-local blocks, each of which is preceded by one 3×3 convolution with stride 2; we adopt a stride of 2 for the transition convolution layer bridging the embedding module and the backbone. In the Non-local block, the addition

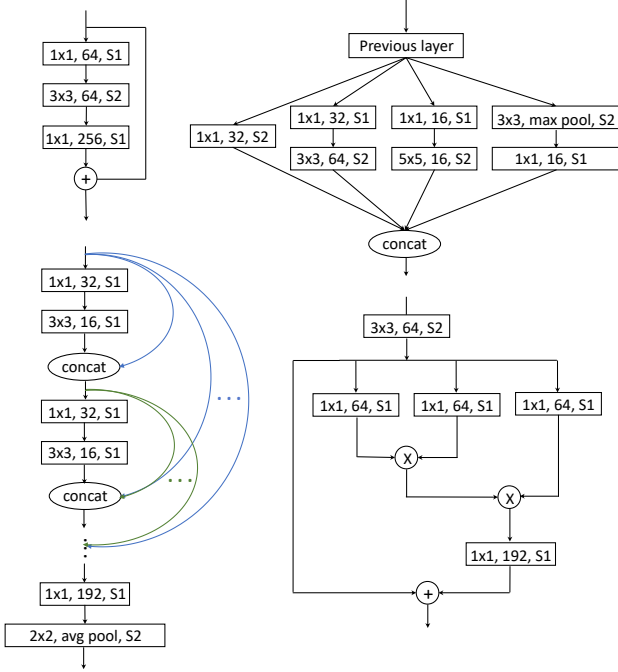


Figure S-3: Illustration of different type of convolution blocks in the *stage* of our module for visual token embedding. Left top: ResNet block; right top: Inception block; left bottom: DenseNet block; right bottom: Non-local block.

(+) and all 1×1 convolutions but the one right before the addition are each followed a BN layer.

D. Additional experiments

D.1. Second-order pooling for T2T-ViT

For the network input, T2T-ViT [S-16] proposes a tokens-to-token module for improving visual token embedding. Here we evaluate how it will perform when combined with our second-order pooling. Specifically, for T2T-ViT, we perform cross-covariance pooling for the output of the last transformer block, and the resulting second-order representation is integrated with that of the class token for classification. We denote the T2T-ViT models without and with second-order pooling by T2T-ViT (w/o) and T2T-ViT (w/), respectively. The experimental settings are same as those described in Sec. 5.1 of the main manuscript.

From Tab. S-7, it can be seen that the accuracy of T2T-ViT (w/) is 4.66% higher than that of T2T-ViT (w/o). We attribute this performance improvement to the integration of the second-order representation of the high-level visual tokens. We also note that the gap between So-ViT (w/) and So-ViT (w/o) is 4.53%. The two gaps (i.e., 4.66% and 4.53%) suggest that our second-order pooling can *consis-*

Method	2nd-order cross-cov pool	Top-1 (%)	Params (M)	TFLOPs (G)	Speed (Hz)
T2T-ViT [S-16]	×	67.20	4.25	0.81	2133
	✓	71.86	6.32	0.81	2016
So-ViT	×	70.40	4.28	0.88	2415
	✓	74.93	6.36	0.88	2370

Table S-7: Results of T2T-ViT and So-ViT with or without second-order pooling.

Method	Type of 2nd-order pool	Norm	Dim.	Top-1 (%)	Speed (Hz)
So-ViT	Covariance matrix (XX^T)	iSQRT* [S-14]	2080	74.04	2332
	Cross-covariance matrix (XY^T)	$\hat{S}\hat{V}$ PN	2048	74.93	2370

Table S-8: Comparison with matrix power normalized covariance pooling. *iSQRT is a fast version of MPN.

tently improve different ViT variants. The experiment here indicates that our classification paradigm, which integrates high-level visual tokens with class token, can well generalize to other transformer models (e.g., T2T-ViT).

D.2. Comparison with MPN

As described in the main manuscript, the proposed cross-covariance pooling produces general square (not necessarily symmetric or positive definite) or non-square matrices, which MPN [S-14] can not be applied to. In order to compare with MPN, we adopt covariance pooling for visual tokens. Specifically, we use a single linear projection which maps the visual tokens to a low dimension (64); then we compute a covariance matrix as global image representation, integrated with the representation of class token for classification. We use the fast version of MPN, i.e., iterative matrix square root normalization (iSQRT) [S-14], to normalize the covariance matrix. We vectorize the upper triangular part of the normalized covariance matrix (due to symmetry), achieving a 2080-dimensional image representation. We use the same experimental settings as Sec. 5.1.

Note that both pooling methods have almost the same parameters (~ 6.4 M) and TFOPS (~ 0.88 G). As can be seen in Tab. S-8, the cross-covariance pooling with $\hat{S}\hat{V}$ PN outperforms the covariance pooling with MPN by $\sim 0.9\%$. This suggests that our cross-covariance pooling has better ability of representation learning. It is also worth mentioning that iSQRT introduces additional memory footprint [S-14, Appendix] while our method brings negligible one.

References

- [S-1] Martín Abadi, Ashish Agarwal, Paul Barham, Eugene Brevdo, Zhifeng Chen, Craig Citro, Greg S. Corrado,

Andy Davis, and et al. TensorFlow: Large-scale machine learning on heterogeneous systems, 2015. Software available from tensorflow.org.

- [S-2] Christopher Bishop. *Pattern Recognition and Machine Learning*. Springer, 2006.
- [S-3] Christopher S. Bretherton, Catherine Smith, and John M. Wallace. An intercomparison of methods for finding coupled patterns in climate data. *Journal of Climate*, (6):541–560, 1992.
- [S-4] Gene H. Golub and Charles F. Van Loan. *Matrix Computations (4th Ed.)*. Johns Hopkins University Press, USA, 2003.
- [S-5] John A Gubner. *Probability and Random Processes for Electrical and Computer Engineers*. Cambridge University Press, 2006.
- [S-6] Kaiming He, Xiangyu Zhang, Shaoqing Ren, and Jian Sun. Deep residual learning for image recognition. In *CVPR*, 2016.
- [S-7] Gao Huang, Zhuang Liu, Laurens Van Der Maaten, and Kilian Q Weinberger. Densely connected convolutional networks. In *CVPR*, 2017.
- [S-8] Catalin Ionescu, Orestis Vantzos, and Cristian Sminchisescu. Training deep networks with structured layers by matrix backpropagation. *arXiv:1509.07838*, 2015.
- [S-9] Yangqing Jia, Evan Shelhamer, Jeff Donahue, Sergey Karayev, Jonathan Long, Ross Girshick, Sergio Guadarrama, and Trevor Darrell. Caffe: Convolutional architecture for fast feature embedding. *arXiv:1408.5093*, 2014.
- [S-10] Adam Paszke, Sam Gross, Francisco Massa, Adam Lerer, James Bradbury, Gregory Chanan, Trevor Killeen, Zeming Lin, Natalia Gimelshein, and et al. Pytorch: An imperative style, high-performance deep learning library. In *NeurIPS*. 2019.
- [S-11] Christian Szegedy, Vincent Vanhoucke, Sergey Ioffe, Jon Shlens, and Zbigniew Wojna. Rethinking the inception architecture for computer vision. In *CVPR*, 2016.
- [S-12] Viivi Uurtio, João M. Monteiro, Jaz Kandola, John Shawe-Taylor, Delmiro Fernandez-Reyes, and Juho Rousu. A tutorial on canonical correlation methods. *ACM Comput. Surv.*, 50(6), 2017.
- [S-13] Hans von Storch and Francis W. Zwiers. *Statistical Analysis in Climate Research*. Cambridge University Press, 2003.
- [S-14] Qilong Wang, Jiangtao Xie, Wangmeng Zuo, Lei Zhang, and Peihua Li. Deep CNNs meet global covariance pooling: Better representation and generalization. *IEEE TPAMI*, 2020.
- [S-15] Xiaolong Wang, Ross Girshick, Abhinav Gupta, and Kaiming He. Non-local neural networks. In *CVPR*, 2018.
- [S-16] Li Yuan, Yunpeng Chen, Tao Wang, Weihao Yu, Yujun Shi, Francis Tay, Jiashi Feng, and Shuicheng Yan. Tokens-to-token ViT: Training vision transformers from scratch on ImageNet. *arXiv:1607.08022*, 2021.